Overload Clutch with Integrated Torque Sensing and Decoupling Detection for Collision Tolerant Hybrid High-Speed Industrial Cobots

Frederik Ostyn[1], Bram Vanderborght[2], and Guillaume Crevecoeur[1]

***Abstract*— A hybrid high-speed industrial collaborative robot can switch between collaborative mode and high-speed mode, combining the advantages of both. While promising, this concept comes with some challenges such as dealing with collisions at high speed. An overload clutch with integrated torque sensing and clutch decoupling detection is presented as enabling technology. Both joint torque sensing and clutch decoupling detection are realized with the same capacitive measurement hardware that consists of paired electrodes. A prototype device is experimentally validated through comparison with a reference torque sensor.**

I. Introduction

Two distinct types of robotic manipulators are commonly found in industry as shown in Fig. 1. High-speed robots excel at executing repeatable tasks at high speed. They operate in cages for safety reasons. Their environment is structured to minimize the risk of collisions that could damage the robot's hardware. Cobots on the other hand move slower but allow collaboration with human operators. They are lightweight [1] and capable of detecting and reacting to collisions [2] based on torque sensing embedded in the joints [3].

A robot capable of switching between high-speed and collaborative mode combines the advantages of both categories. It has the potential to collaborate safely with humans at low speed while allowing high production throughput otherwise, i.e. when humans are not in the vicinity of the robot. Which mode the robot is in can e.g. be decided by safety scanners or light guards. ABB's SWIFTY [4], Yaskawa's HC20DTP [5] and Comau's Racer-5-0.80 [6] are recent industrial examples of this trend towards Hybrid High-Speed Cobots (HHSC).

As humans are allowed in the vicinity of the robot in low-speed mode, the environment in which the robot operates becomes less structured. The latter increases the risk of collision which can result in catastrophic failure of the robot hardware in high-speed mode. Protecting the robot during a collision through overload clutching [7] is hence particularly relevant for HHSCs.

A. Overload clutches and decoupling detection

Two major types of overload clutches exist: friction clutches (FC) and cam clutches (CC). In the former, both clutch halves are locked through a (friction) force closure. When they recouple, the original relative position between the input and output flange is lost. Recalibration is required to retrieve the original kinematic configuration of the joints. Examples are [8]–[10]. Cam clutches such as [11]–[13] on the other hand are locked through form closure. They can be designed to have a unique relative position of the input and output flanges. The residual torque that remains after decoupling is however insufficient to keep the robot upright.

The Combined Friction Cam Clutch (CFCC) proposed in [7] combines both principles in a torque-dense design. By design, the CFCC has a threshold torque τ_{TH} smaller or equal to the maximum allowed torque of the drivetrain, hence protecting e.g. the strainwave gear. It has a unique relative position between the input and output clutch flanges and has significant residual torque. Detecting clutch decoupling was shown to be important in order not to overstretch the clutch by braking upon clutch decoupling. An external inductive sensor was used a.o. in [14].

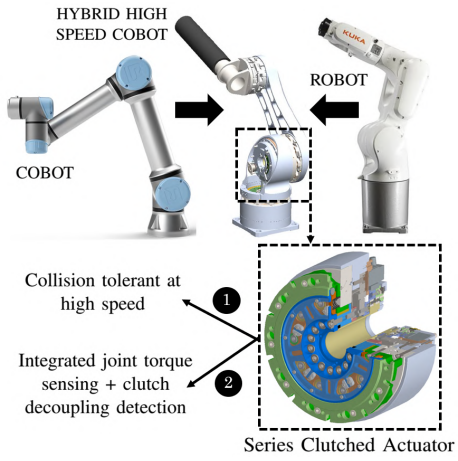

Fig. 1: A Hybrid High Speed Cobot (HHSC) is capable of switching between high-speed and collaborative mode. A custom three axis HHSC equipped with series clutched actuators is shown. This paper presents the development of an overload clutch with integrated joint torque sensing and clutch decoupling detection. It protects the robot's hardware during a collision while enabling cobot functionality.

B. Joint torque sensing

Multiple joint torque sensor technologies exist. The most common ones rely on strain gauges as in [3] and [15] or capacitive sensing as in [16]–[18]. Strain gauge sensor technology is mature but not cheap. Strain gauges them-

This work was supported by the BOF project 01N02716.

[1]F. Ostyn and G. Crevecoeur are with the Department of Electromechanical, Systems and Metal Engineering, Ghent University, 9000 Ghent, Belgium; and with the Core Lab EEDT-DC, Flanders Make, 3920 Lommel, Belgium (e-mail: frederik.ostyn@ugent.be.)

[2]B. Vanderborght is with the Robotics and Multibody Mechanics (R&MM) Research Group, Vrije Universiteit Brussel (VUB), 1050 Brussels, Belgium; with Imec and with the Core Lab R&MM, Flanders Make, 3920 Lommel, Belgium.

selves are not necessarily expensive but they require manual and precarious installation. Joint torque sensing based on capacitive measurements is an interesting alternative. The main advantage is that besides a grounded deformable base structure, only a Printed Circuit Board (PCB) with electrodes is required. In [16], Choi *et al.* demonstrated this concept. They extended the technology towards 6-axis force and torque sensing and incrementally increased the sensitivity of the capacitive measurements by adding PCB edge plating and adding wedges to the grounded base structure [17]. Kim *et al.* presented a different design with a focus on the deformable base structure [18].

Integrating sensing in the clutch has several advantages. First of all, the sensor is by design protected from overload. Furthermore, the added weight, volume and cost will be reduced with respect to two separate devices (clutch versus sensor) in series. Kang *et al.* integrated small-sized pressure sensors in their Spring-Clutch design to realise a passive and active safe robotic joint [19]. Their device is however designed to protect human operators during a collision and relies on a gravity compensator to reduce the clutch threshold torque. The CFCC used in this article has a higher threshold, has higher torque density and serves to protect the robot itself.

C. Contribution and outline

A clutch tailored to HHSCs is presented in this article. Beside overload protection, both clutch decoupling detection and joint torque sensing are integrated. It is a key part of a three degrees of freedom collision tolerant HHSC with Series Clutched Actuators [10], [20] currently under development (Fig. 1). The particular contribution of this article lies in the capacitive measurement hardware consisting of paired electrodes to distinguish between torque sensing and clutch decoupling detection. By sharing hardware, a compact instrumented clutch is obtained.

This article continues with the working principle (Section II), the mechanical and the electronic design (Sections III–IV) of the CFCC with integrated sensing. The design is calibrated and experimentally verified in Section V and discussed in Section VI. Section VII summarizes the findings.

II. Working principle

Figure 2(a) shows a schematic representation of a CFCC with integrated joint torque sensing and clutch decoupling detection. The clutch consists of an output (1, green) and an input flange (2, blue). The input flange is split in two inertias connected through a torsion spring (6). The latter is not necessarily a separate physical element but could also be the inherent compliance of the input flange.

A. Combined Friction Cam Clutch

In the coupled or locked state, torque can be transferred between both flanges through a force and form closure. The force closure is realised through friction generated between (1) and (2) and between (2) and (3) by the preloaded springs (4). The form closure is due to elements (3, orange) which

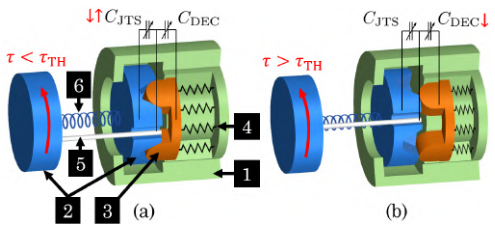

Fig. 2: Working principle of the Combined Friction Cam Clutch with integrated joint torque sensing and clutch decoupling detection. The coupled and decoupled clutch are respectively shown in (a) and (b).

are pushed in the recesses of (2) which acts as cam plate. The same set of springs (4) is used to pretension the cam assembly which results in a torque dense design.

If a torque larger than the threshold torque $\tau > \tau_{\mathrm{TH}}$ is applied to the input flange, decoupling happens. The elements (3) leave the recesses of cam (2) and springs (4) are compressed as shown in Fig. 2(b). The decoupled clutch can still transfer a significant residual torque through friction. The latter is the first important property of a CFCC and allows to keep the robot arm upright, even in decoupled state. With zero residual torque, the robot would collapse due to its own weight [7]. The second important property is that the cam mechanism is designed as such to allow recoupling only in the same relative position between input and output flange as before decoupling.

B. Integrated Sensing

Due to the torsion spring, the input flange inertias rotate with respect to each other when loaded. This displacement results in a changing capacitance C_{JTS} between the input flange inertia on the right and an electrode (5), mechanically fixed but electrically isolated from the input flange inertia on the left. By measuring the change in capacitance C_{JTS}, the torque transmitted between the input and output flange can be estimated.

A second capacitance C_{DEC} in parallel with C_{JTS} exists between the electrode and the spring plate. As they are in parallel, the total capacitance is $C_{\mathrm{JTS}} + C_{\mathrm{DEC}}$. By decoupling, C_{DEC} significantly drops which can be used as detection for this event. C_{JTS} will not necessarily render accurate joint torque readings in decoupled state.

III. Mechanical design

This working principle is translated to an actual mechanical design that can be integrated in the series clutched actuator mentioned in the introduction. The design shown in Fig. 3(a-b) resembles a spoked wheel with the number of spokes and their dimensions as key design parameters. The color code is similar as in Fig. 2. The robot arm is attached to the green output flange (1). The blue input flange (2) is connected to the output of a strain wave reducer. Both flanges can rotate with respect to each other due to sliding bearing (5). The outer ring of the cross roller bearing (6) is fixed. The spokes (11) that connect the inner and outer ring of (2)

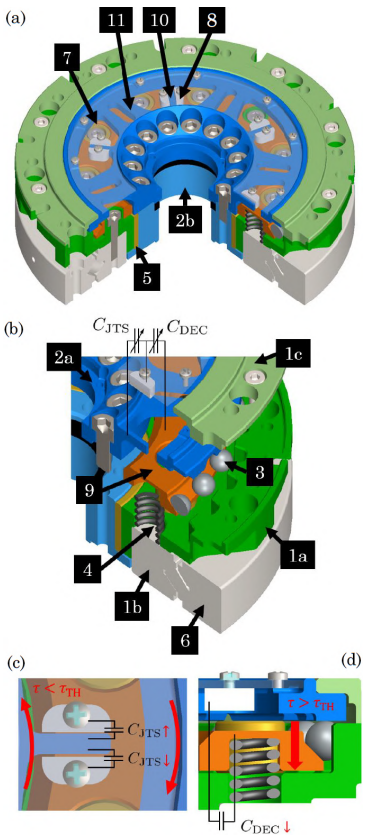

Fig. 3: Cross sectional (a) and exploded (b) views of the overload clutch with integrated sensing. The different components are detailed in the main text. Joint torque sensing is shown in (c) and decoupling detection in (d).

deform when torque is applied. They are represented by the torsion spring in Fig. 2. The cam elements (3) are pushed by springs (4) and spring plate (9) into the recesses of cam plate (2a). A PCB housing multiple electrodes (8) and the measurement unit is attached to the outer ring of the clutch cam (2a). It is made transparent in Fig. 3 to show the inner structure of the clutch. The electrodes (8) are electrically isolated from the grounded cam (2a). The electrodes face protrusions (10) of the inner ring of (2a). These protrusions do not deform themselves but follow the rotation of the inner with respect to the outer ring.

A. *Electrode pairing*

Instead of using a single electrode, the design incorporates multiple electrodes, organised in pairs. The paired electrodes face opposite sides of the protrusions. If torque is transmitted by the clutch, one capacitance C_{JTS} will increase while the capacitance of the paired electrode will decrease and vice versa. By doing so, the required number of protrusions halves. More importantly, electrode pairing allows to distinguish spring plate movement (related to C_{DEC}) from joint torque (related to C_{JTS}). Even in coupled state, the spring plate (3+9) can move slightly as the cam plate (2a) converts the joint torque in a force working on the former. Due to static friction in the linear bearing (7) guiding the spring plate (3+9) up and down, the plate could stick resulting in sensor hysteresis. This parasitic effect can be distinguished from joint torque as the up and down translation of the spring plate respectively increases and decreases C_{DEC} of both paired electrodes equally. Combined with the earlier statement, one gets: if the total electrode capacitance $C_{\mathrm{JTS}}+C_{\mathrm{DEC}}$ of one of the paired electrodes increases while the other one decreases, this can be attributed to joint torque. If on the contrary, the total electrode capacitance $C_{\mathrm{JTS}} + C_{\mathrm{DEC}}$ changes in similar fashion, this will be due to a moving spring plate. This statement has been illustrated in Fig. 3(c-d). In case a torque (red arrow) $\tau < \tau_{\mathrm{TH}}$ is applied, C_{JTS} will change opposite ($\uparrow\downarrow$) for the paired electrodes (Fig. 3(c)). If the clutch decouples and the spring plate is pushed down, the capacitance of both electrodes will decrease similarly ($\downarrow\downarrow$) as shown in Fig. 3(d).

The design has multiple of these electrode pairs in order to average their output. This reduces the noise on the final reading and adds robustness to the sensor. By distributing the electrode pairs over the circumference of the cam, non-uniform loading of the spokes can be taken into account. It could occur for instance that not all the spokes transmit the same torque between the inner and outer ring of cam (2a). Other sources of noise could be related to electromagnetic compatibility. If one of the readings momentarily deviates too much with respect to the others, it can be identified as an outlier and be filtered out. If the faulty reading persists, it can be discarded completely while the sensor continues working. Possibly the operator could be warned of this event.

B. *Finite Element Model*

The design should be optimized according to the trade-off joint sensing accuracy versus strength and torsion stiffness S. The higher the compliance of the spokes, the larger the relative rotation of the inner versus the outer ring upon loading and hence the higher the sensing accuracy. However, the maximum stress in the spokes should not cause material yielding. High dynamic motion should also not be compromised by the added compliance. Given the torsional stiffness of the harmonic drive S_{HD}, the cam's torsional stiffness is chosen $S \geq 3\, S_{\mathrm{HD}}$. By doing so, the actuator's total torsional stiffness would hence be lowered by $\leq 25\%$ by adding the clutch in series.

A finite element model of the cam is constructed to evaluate different mechanical designs. Fig. 4(a-b) shows the calculations for an earlier iteration and (c-d) for the current iteration. The simulation parameters are listed in Table I. These specifications/parameters are for the base and shoulder actuator of the HHSC design presented in Fig. 1. By applying the clutch threshold τ_{TH} –which is the maximum load– it can be verified that the cam will not yield. The torsional stiffness S can be calculated as $S = \tau_{\mathrm{TH}} R_{\mathrm{CFCC}}/U_z$ with U_z the (cartesian) displacement in Fig. 4(b,d) at a radius R_{CFCC} when applying the same load τ_{TH}.

What proved also important is that the outer ring should not deflect too much from a circle upon loading. As the outer ring is clamped through a combination of force and

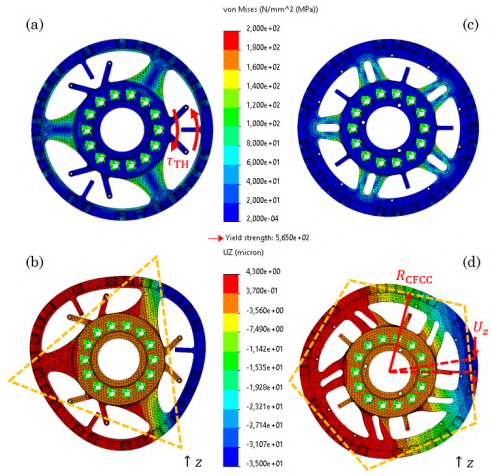

Fig. 4: Finite element modelling of the clutch cam. (a) shows the von Mises stress and (b) the displacement along the Cartesian z-direction for an initial design iteration. (c) and (d) respectively show similar quantities for the current design.

form closure, the deformed shape does not necessarily return completely to its original circular shape. This resulted in sensor hysteresis in an earlier design iteration with three spokes, shown in Fig. 4(a-b). The current design shown in Fig. 4(c-d) has five double spokes and a thicker outer ring which reduced sensor hysteresis considerably. The deflection from a circle is represented by the orange dashed triangle (Fig. 4(b)) and pentagon (Fig. 4(d)). It may be clear that a pentagon resembles a circle more than a triangle.

C. Estimating the capacitance

Due to their rectangular shape, the initial capacitance $C_{\mathrm{JTS},0}$ can be calculated through

$$C_{\mathrm{JTS},0} = \epsilon_0 \epsilon_r \frac{A_{\mathrm{JTS}}}{d_{\mathrm{JTS},0}} = \epsilon_0 \epsilon_r \frac{lh}{d_{\mathrm{JTS},0}} \tag{1}$$

with $\epsilon_0 = 8.854 \times 10^{-12}$ F/m the vacuum permittivity, $\epsilon_r = 1$ the relative permittivity of air, $A_{\mathrm{JTS}} = lh$ the electrode area with l and h its length and height respectively, and $d_{\mathrm{JTS},0}$ the distance between the electrode and the protrusion. Likewise the initial capacitance between the electrode and the grounded spring plate reads

$$C_{\mathrm{DEC},0} = \epsilon_0 \epsilon_r \frac{A_{\mathrm{DEC}}}{d_{\mathrm{DEC},0}} \tag{2}$$

if fringing effects are ignored, with A_{DEC} the bottom surface area of the electrode and $d_{\mathrm{DEC},0}$ the distance between the electrode and the spring plate with in general $d_{\mathrm{DEC},0} >> d_{\mathrm{JTS},0}$.

For a given torsional stiffness S and sensor radius R_{JTS}, the maximum displacement of the protrusions on the inner ring and the electrodes, mechanically attached but electrically isolated to the outer ring can be approximated by $\Delta d_{\mathrm{JTS}} = \tau_{\mathrm{TH}} R_{\mathrm{JTS}} / S$. The resulting maximum change in joint torque

TABLE I: Design parameters for CFCC with integrated sensing.

Specification/parameter	Symbol	Unit	Value
Threshold torque	τ_{TH}	Nm	240
Sensor compliance	S	kNm/rad	400
CFCC radius	R_{CFCC}	mm	62.5
JTS radius	R_{JTS}	mm	42.0
Electrode length	l	mm	10.0
Electrode height	h	mm	4.5
Electrode bottom area	A_{DEC}	mm^2	34
Initial distance electrode-protrusion	$d_{\mathrm{JTS},0}$	mm	0.15
Initial distance electrode-spring plate	$d_{\mathrm{DEC},0}$	mm	1.5
Spring plate translation	Δd_{DEC}	mm	2.5
Initial capacitance el.-protrusion	$C_{\mathrm{JTS},0}$	pF	2.67
Initial capacitance el.-spring plate	$C_{\mathrm{DEC},0}$	pF	0.20
Joint torque capacitive change	ΔC_{JTS}	pF	0.46
Decoupling capacitive change	ΔC_{DEC}	pF	0.13
Calculated resolution	τ_{res}	Nm	0.18

capacitance is hence:

$$\begin{aligned}\Delta C_{\mathrm{JTS},\pm} &= \epsilon_0 \epsilon_r lh \left(\frac{1}{d_{\mathrm{JTS},0}} - \frac{1}{d_{\mathrm{JTS},0} \pm \Delta d_{\mathrm{JTS}}} \right) \\ &= C_{\mathrm{JTS},0} \left(\pm \frac{\Delta d_{\mathrm{JTS}}}{d_{\mathrm{JTS},0}} - \left[\frac{\Delta d_{\mathrm{JTS}}}{d_{\mathrm{JTS},0}} \right]^2 + \text{H.O.T.} \right)\end{aligned} \tag{3}$$

with $\pm$ depending on which of the paired electrodes is considered and with the latter equality expanded as Taylor series. By averaging over a sensor pair (assuming the same $C_{\mathrm{JTS},0}$), the second order terms cancel:

$$\begin{aligned}\Delta C_{\mathrm{JTS}} &= \frac{1}{2}(\Delta C_{\mathrm{JTS},+} - \Delta C_{\mathrm{JTS},-}) \\ &= C_{\mathrm{JTS},0} \left(\frac{\Delta d_{\mathrm{JTS}}}{d_{\mathrm{JTS},0}} + \left[\frac{\Delta d_{\mathrm{JTS}}}{d_{\mathrm{JTS},0}} \right]^3 + \text{H.O.T.} \right)\end{aligned} \tag{4}$$

When approximating $\Delta C_{\mathrm{JTS},\pm} \approx \pm C_{\mathrm{JTS},0} \Delta d_{\mathrm{JTS}} / d_{\mathrm{JTS},0}$, the averaged capacitance ΔC_{JTS} is hence proportional with the applied torque, while the error is only of third order. This linear approximation will simplify sensor calibration considerably.

The change in capacitance due to decoupling can be calculated with

$$\Delta C_{\mathrm{DEC}} = \epsilon_0 \epsilon_r A_{\mathrm{DEC}} \left(\frac{1}{d_{\mathrm{DEC},0}} - \frac{1}{d_{\mathrm{DEC},0} + \Delta d_{\mathrm{DEC}}} \right) > 0 \tag{5}$$

with Δd_{DEC} the translation of the spring plate when decoupling the clutch.

IV. Electronic Design

The electronic design is shown in Fig. 5. A custom PCB houses two Analog Devices AD7147 Capacitance-to-Digital-Converters (CDC) each measuring four different capacitances (two sensor pairs). These are read through a Serial Peripheral Interface (SPI) by a microcontroller (MCU) where they are post-processed. The electrodes are shielded from ground according to the manufacturer's recommendations.

The AD7147 has a 15 bit precision and a resolution of $C_{\mathrm{res}} = 3.5 \times 10^{-4}$ pF in a range of ± 8 pF. The theoretical accuracy of the joint torque sensor is hence $\tau_{\mathrm{res}} = \tau_{\mathrm{TH}} C_{\mathrm{res}} / \Delta C_{\mathrm{JTS}}$ for which the numerical value is listed in Table I.

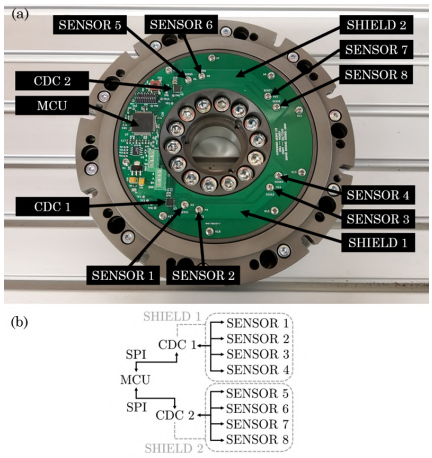

Fig. 5: (a) Actual clutch with electronics; (b) Schematic of the electronics.

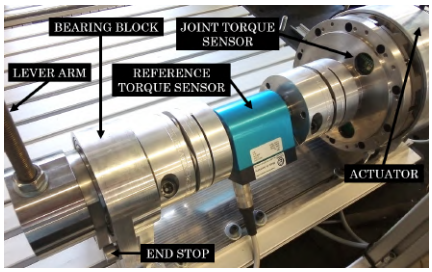

Fig. 6: Overview of the experimental setup. Shown in series are the actuator with integrated sensing, a reference sensor, bearing block and a lever arm to apply external torque.

V. Experimental Proof of Concept

In this section, a setup is proposed that allows to benchmark the joint torque sensing capability of the custom integrated sensor with respect to a reference sensor. The detection of decoupling and recoupling of the clutch are evaluated as well as the effect of the latter on the joint torque sensing accuracy.

A. Experimental setup

The experimental setup shown in Fig. 6 consists of a clutched actuator with the proposed integrated sensor in series with a Lorentz Messtechnik DR-2112-R 500 Nm reference joint torque sensor. A lever arm is attached at the other end which allows to apply external load by hand. The rotation of the actuator is limited by two end stops. If the motor is instructed to go beyond either end stop, the clutch decouples.

B. Joint torque sensor calibration

The joint torque sensor is calibrated by comparing the raw CDC sensor data $\tau_{\mathrm{CDC,i}}$ of the i–th CDC with the reference joint torque sensor data. Assuming a linear dependence (as motivated in Section III.C), standard linear least squares techniques [21] can be used to find the optimal offset α_i and slope β_i:

$$\tau_{\mathrm{cal,i}} = \beta_i(\tau_{\mathrm{CDC,i}} - \alpha_i) \tag{6}$$

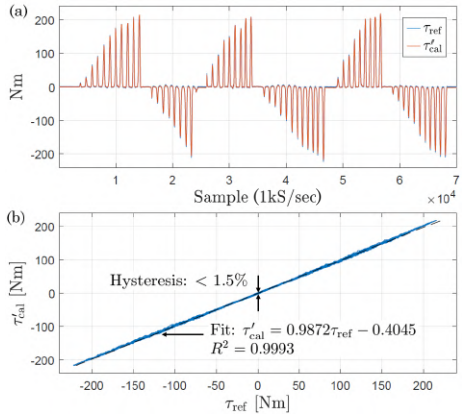

Fig. 7: Calibration of the joint torque sensor. (a) joint torque profile; (b) the calibrated torque τ'_{cal} as function of τ_{ref} with linear fit.

minimizing the error $||\tau_{\mathrm{ref}} - \tau_{\mathrm{cal,i}}||_2^2$. Note that β_i can be larger or smaller than zero. Each CDC pair (i, j) will have $\beta_i\beta_j < 0$ as the capacitance increases upon loading for one of the CDCs and decreases for the other.

Fig. 7 shows the result of such a calibration procedure. On top are the readings of the reference joint torque sensor as well as the calibrated and averaged CDC values

$$\tau'_{\mathrm{cal}} = \frac{1}{M}\left(\sum_i^M \beta_i[\tau_{\mathrm{CDC,i}} - \alpha_i]\right) \tag{7}$$

with M the number of CDCs, $M = 8$ in this case. The calculated resolution of 0.18 Nm listed in Table I is reflected in the proportionality constants $|\beta_i|$ which were ranging $0.14 < |\beta_i| < 0.28$ and 0.21 on average. On the bottom of Fig. 7, the calibrated signal τ'_{cal} is plotted as function of the reference torque τ_{ref}. A linear fit $\tau'_{\mathrm{cal}} = \delta\tau_{\mathrm{ref}} + \epsilon$ is found with proportionality $\delta = 0.9872$ and offset $\epsilon = -0.4045$ Nm. The calibration of Eq. (7) is extended to

$$\tau_{\mathrm{cal}} = \frac{1}{\delta}\left[\frac{1}{M}\left(\sum_i^M \beta_i[\tau_{\mathrm{CDC,i}} - \alpha_i]\right) - \epsilon\right] \tag{8}$$

to take into account $\delta \neq 1$ and $\epsilon \neq 0$ Nm. A hysteresis $< 1.5\%$ of the maximum sensor torque τ_{TH} is found.

C. Clutch decoupling detection

Fig. 8 shows an experiment with three consecutive stages. In the first stage, an external load is applied on the lever arm. The applied torque is representative for human-robot collaboration. In the second stage, the actuator is instructed to move beyond the end stop resulting in clutch decoupling. As seen in Fig. 8, the torque increases first towards the clutch threshold. Beyond this threshold, the clutch decouples. The spring plate is pushed down which results in opposite calibrated readings of the odd and even CDCs given $\beta_i\beta_j < 0$ for electrode pair (i, j). Clutch decoupling can hence clearly be distinguished from joint torque. While decoupled, the joint torque as measured by the CDCs may not be viable as the calibration of the sensor might not be valid

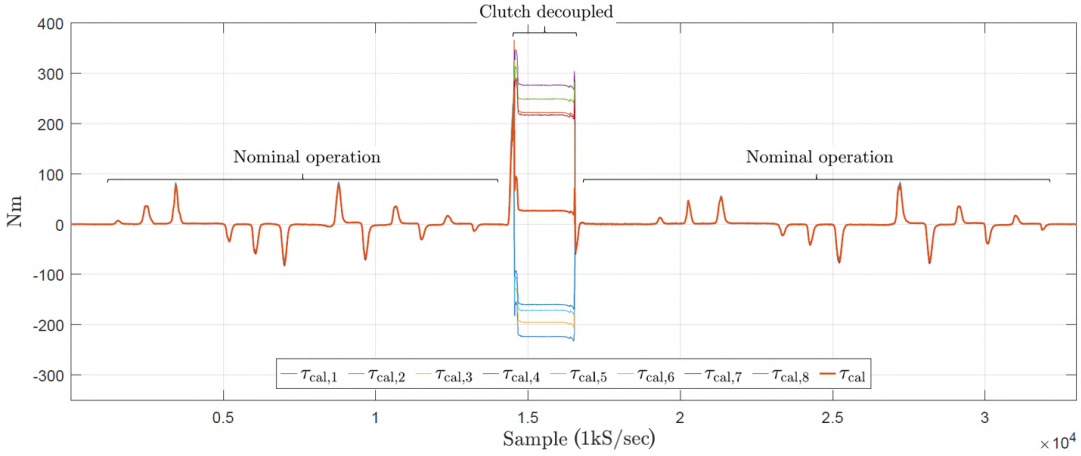

Fig. 8: Output for the individual calibrated CDCs as well as their average.

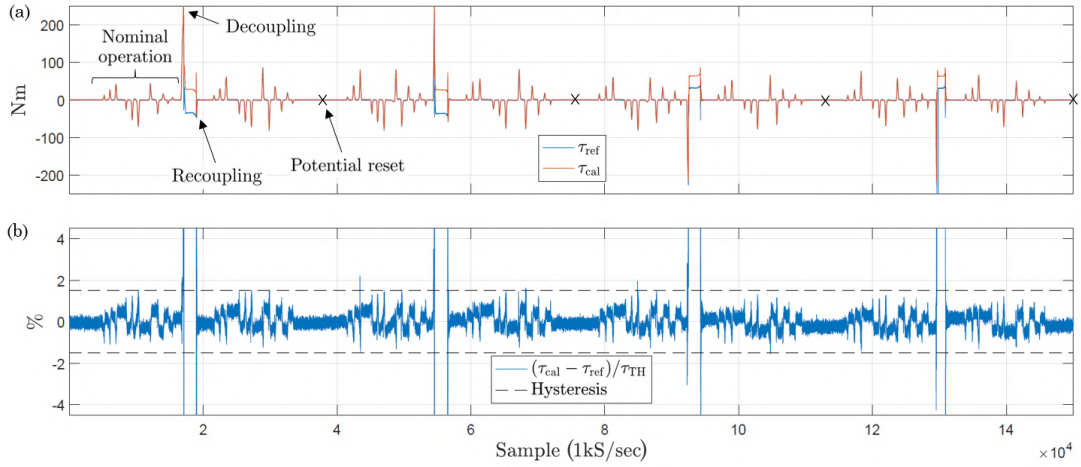

Fig. 9: Four consecutive experiments of external loading alternated with de- and recoupling the clutch; (a) shows both the reference and calibrated torque and (b) the error as percentage of the threshold torque τ_{TH}.

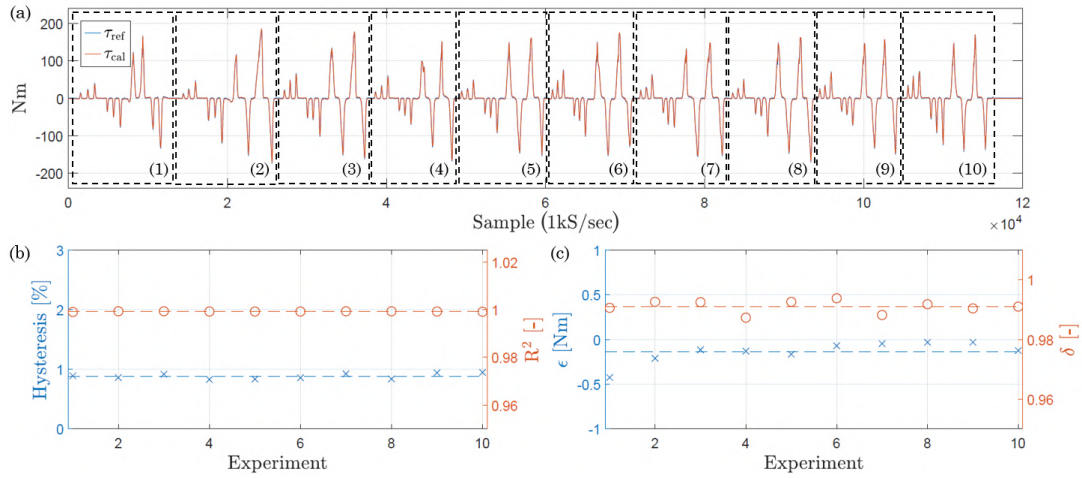

Fig. 10: (a) Ten consecutive experiments without clutch decoupling; (b) plot of the hysteresis and coefficient of determination R^2 for a linear fit of each of the experiments; (c) plot of the proportionality δ and offset ϵ for a linear fit of each of the experiments.

in decoupled state. After recoupling, external load is applied in similar fashion as in the first stage.

Fig. 9(a) shows four consecutive decoupling experiments. The clutch is decoupled twice in either rotation direction. Fig. 9(b) shows the error in percentage of the threshold torque τ_{TH}. Note that this error is mainly due to sensor hysteresis. No significant additional offset is measured in this experiment due to de- and recoupling.

D. Drift

In order to study if there is joint torque sensor drift in nominal operation due to its integration in the clutch, ten consecutive measurements were performed as shown in Fig 10(a). A linear fit was made and the resulting parameters are listed in Fig. 10(b-c). Note that no significant drift in any of the parameters is experimentally observed.

VI. Discussion

The experiments presented above prove that it is possible to integrate both clutch decoupling detection as well as joint torque sensing in an overload clutch. Some important remarks:

1) In order to increase robustness, the proper working of the sensor could be checked after de- and recoupling the clutch. A procedure could be implemented to position the robot in a reference kinematic configuration where the joint torques are known (e.g. because they were measured in this configuration prior to clutch decoupling). If one or several of the individual CDC readings are out of tolerance, they could be reset. This procedure would not require recalibration with respect to a reference sensor, nor is there a need for human operator intervention. Potential reset points are indicated in Fig. 9(a).
2) The most challenging issue seems to be further reducing sensor hysteresis. As stated in Section III.B, upon deforming the cam, it deflects from the original shape and not necessarily returns to this shape due to the complex boundary condition of the CFCC. Reducing sensor hysteresis through design optimization of the cam or through compensation in software is considered to be future work.

VII. Conclusion

A hybrid high-speed cobot combines the advantages of high production throughput in absence of humans and collaboration at lower speed. This paper presents an overload clutch tailored to this robot type. Joint torque sensing and clutch decoupling detection are integrated in the clutch. Both features are realised relying on capacitive measurements and a paired electrode architecture. Joint torque is distinguished from clutch decoupling as the former results in an opposite capacitance change in the electrode pair while the latter changes the capacitance equally. This was demonstrated by including the prototype clutch in a custom series clutched actuator and purpose built test bench including a reference torque sensor.

References

[1] A. Albu-Schäffer, O. Eiberger, M. Grebenstein, S. Haddadin, C. Ott, T. Wimböck, S. Wolf, and G. Hirzinger. Soft robotics: From torque feedback controlled lightweight robots to intrinsically compliant systems. *IEEE Robotics and Automation Magazine*, 15:20–30, 01 2008.

[2] S. Haddadin, A. Luca, and A. Albu-Schaffer. Robot collisions: A survey on detection, isolation, and identification. *IEEE Transactions on Robotics*, PP:1–21, 10 2017.

[3] I. Kim, H. Kim, J. Song. Design of Joint Torque Sensor and Joint Structure of a Robot Arm to Minimize Crosstalk and Torque Ripple *International Conference on Ubiquitous Robots and Ambient Intelligence (URAI)*, 2012.

[4] ABB Swifty. `https://library.e.abb.com`. Accessed: 26.08.2022.

[5] Yaskawa HC20DTP. `https://www.motoman.com`. Accessed: 26.08.2022.

[6] Comau Racer-5-0.80 Cobot. `https://www.comau.com`. Accessed: 26.08.2022.

[7] F. Ostyn, T. Lefebvre, B. Vanderborght, and G. Crevecoeur. Overload clutch design for collision tolerant high–speed industrial robots. *IEEE Robotics and Automation Letters*, 6(2):863–870, 4 2021.

[8] H. Terada, M. Kobayashi, and K. Imase. Development of a trochoidal gear reducer with a slipping rollers type torque limiter. In *New Advances in Mechanisms, Transmissions and Applications*, pages 49–56. Springer Netherlands, 2014.

[9] N. Imamura, A. Sato, A. Yoshida, and K. Nagamura. A new–type torque limiter with friction adjusting mechanism for robots. In *World Congress in Mechanism and Machine Science*, pages 19–25, 2011.

[10] N. Lauzier and C. Gosselin. Series clutch actuators for safe physical human-robot interaction. In *2011 IEEE International Conference on Robotics and Automation*, pages 5401–5406, 2011.

[11] R. Kang, H. Liu, F. Meng, R. Zhang, X. Ma, B. Liu, A. Ming, and Q. Huang. An overload protector inspired by joint dislocation and reduction for shoulder of humanoid robot. In *2018 IEEE International Conference on Robotics and Biomimetics (ROBIO)*, pages 2019–2024, 12 2018.

[12] X. Guo, W. Zhang, H. Liu, Z. Yu, W. Zhang, W. Conus, K. Hashimoto, and Q. Huang. A torque limiter for safe joint applied to humanoid robots against falling damage. In *2015 IEEE International Conference on Robotics and Biomimetics (ROBIO)*, pages 2454–2459, 2015.

[13] W. Lee, J. Choi, and S. Kang. Spring-clutch: A safe torque limiter based on a spring and cam mechanism with the ability to reinitialize its position. In *2009 IEEE/RSJ International Conference on Intelligent Robots and Systems*, pages 5140–5145, 2009.

[14] F. Ostyn, B. Vanderborght, and G. Crevecoeur. Comparison of Collision Detection Techniques for High-Speed Industrial Robot Actuators with Overload Clutch *IEEE/ASME International Conference on Advanced Intelligent Mechatronics (AIM)*, 2021.

[15] N. Hendrich, F. Wasserfall, J. Zhang. 3D Printed Low-cost Force-Torque Sensors *IEEE Access*, 8:140569–140585, 2020.

[16] Y. Kim, U. Kim, D. Seok, J. So, H. Choi. Design of Novel Capacitive type Torque Sensor for Robotic Applications *International Conference on Ubiquitous Robots and Ambient Intelligence (URAI)*, 2016.

[17] D. Seok, Y. Kim, S. Lee, J. Kim, H. Choi. Ultra-Thin Joint Torque Sensor With Enhanced Sensitivity for Robotic Application *IEEE Robotics and Automation Letters*, 5(4):5873–5880, 10 2020.

[18] J. Kim, H. Jeon, Y. Jeong, Y. Kim. High Stiffness Capacitive Type Torque Sensor with Flexure Structure for Cooperative Industrial Robots *International Conference on Ubiquitous Robots and Ambient Intelligence (URAI)*, 2017.

[19] D. Choi, G. Yang, J. Choi, W. Lee, C. Cho, and S. Kang. A Safe Joint with a Joint Torque Sensor *International Conference on Ubiquitous Robots and Ambient Intelligence (URAI)*, 2011.

[20] Z. Niu, M. I. Awad, U. H. Shah, M. N. Boushaki, Y. Zweiri, L. Seneviratne and I. Hussain. Towards Safe Physical Human-Robot Interaction by Exploring the Rapid Stiffness Switching Feature of Discrete Variable Stiffness Actuation. In *IEEE Robotics and Automation Letters*, 7(3):8084–80910, 07 2022.

[21] L. Ljung. System identification: theory for the user *Prentice-Hall*, 1999.